Virginia Commonwealth University
VCU Scholars Compass

Statistical Sciences and Operations Research Publications

Dept. of Statistical Sciences and Operations Research

2015

Firing Rate Dynamics in Recurrent Spiking Neural Networks with Intrinsic and Network Heterogeneity

Cheng Ly
Virginia Commonwealth University, cly@vcu.edu

Follow this and additional works at: http://scholarscompass.vcu.edu/ssor_pubs

Part of the Computational Neuroscience Commons, Non-linear Dynamics Commons, Other Applied Mathematics Commons, Other Statistics and Probability Commons, and the Systems Neuroscience Commons

Downloaded from
http://scholarscompass.vcu.edu/ssor_pubs/13

This Article is brought to you for free and open access by the Dept. of Statistical Sciences and Operations Research at VCU Scholars Compass. It has been accepted for inclusion in Statistical Sciences and Operations Research Publications by an authorized administrator of VCU Scholars Compass. For more information, please contact libcompass@vcu.edu.

Journal of Computational Neuroscience manuscript No.
(will be inserted by the editor)

Firing Rate Dynamics in Recurrent Spiking Neural Networks with Intrinsic and Network Heterogeneity

Cheng Ly

Received: date / Accepted: date

Abstract Heterogeneity of neural attributes has recently gained a lot of attention and is increasing recognized as a crucial feature in neural processing. Despite its importance, this physiological feature has traditionally been neglected in theoretical studies of cortical neural networks. Thus, there is still a lot unknown about the consequences of cellular and circuit heterogeneity in spiking neural networks. In particular, combining network or synaptic heterogeneity and intrinsic heterogeneity has yet to be considered systematically despite the fact that both are known to exist and likely have significant roles in neural network dynamics. In a canonical recurrent spiking neural network model, we study how these two forms of heterogeneity lead to different distributions of excitatory firing rates. To analytically characterize how these types of heterogeneities affect the network, we employ a dimension reduction method that relies on a combination of Monte Carlo simulations and probability density function equations. We find that the relationship between intrinsic and network heterogeneity has a strong effect on the overall level of heterogeneity of the firing rates. Specifically, this relationship can lead to amplification or attenuation of firing rate heterogeneity, and these effects depend on whether the recurrent network is firing asynchronously or rhythmically firing. These observations are captured with the aforementioned reduction method, and furthermore simpler analytic descriptions based on this dimension reduction method are developed. The final analytic descriptions provide compact and descriptive formulas for how the relationship between intrinsic and network heterogeneity determines the firing rate heterogeneity dynamics in various settings.

Keywords Leaky integrate-and-fire · Recurrent E/I Network · Intrinsic Heterogeneity · Network Heterogeneity · Dimension Reduction

1 Introduction

Theoretical studies of spiking neuronal networks have been extremely valuable for experimentalists and theoreticians. Uncovering the underlying mechanisms of complex phenomena in neural circuits often requires theory and/or computation. In this vein, this paper focusses on the effects of heterogeneous neural attributes in model neural networks. Heterogeneity is an undeniable physiological feature that has often been ignored in theoretical studies because it complicates theoretical analyses. Not only is there

C. Ly
Department of Statistical Sciences and Operations Research
Virginia Commonwealth University
Richmond, Virginia 23284-3083 USA
Tel.: +1(804) 828-5842
Fax: +(804) 828-8785
E-mail: CLy@vcu.edu

ample experimental evidence for heterogeneity of neural networks at many scales (Markram et al, 1997; Parker, 2003; Marder and Goaillard, 2006; Bremaud et al, 2007), but the importance of heterogeneity in neural computational is becoming more apparent. Indeed, a combination of theoretical and experimental studies on neural networks have demonstrated the value of heterogeneity (Ostojic et al, 2009; Hermann and Touboul, 2012). In particular, theoretical studies have shown that heterogeneity can generally lead to efficient neural coding (Shamir and Sompolinsky, 2006; Chelaru and Dragoi, 2008; Padmanabhan and Urban, 2010; Marsat and Maler, 2010; Mejias and Longtin, 2012; Tripathy et al, 2013). However, there is still not a lot known about heterogeneity. Specifically, how do different sources of heterogeneity interact and lead to different neural network activity?

We make a distinction between different sources of heterogeneity, addressing two forms: intrinsic and network heterogeneity, both of which are known to exist. Intrinsic heterogeneity are differences due to cellular properties that exist without coupling to other neurons (Marder and Goaillard, 2006; Padmanabhan and Urban, 2010), for example the membrane time constant, threshold for spiking, reversal potentials, etc. Network heterogeneity, that is heterogeneity induced by coupling in a neural network, can arise from differences in synaptic coupling between neurons (Parker, 2003; Marder and Goaillard, 2006; Bremaud et al, 2007; Oswald et al, 2009). To the best of our knowledge, the physiological relationship between these two sources of heterogeneity are not known. Therefore, we systematically study the effects of these forms of heterogeneity on a canonical recurrent spiking neural network. The main motivation for studying the relationship between different heterogeneous components is to provide a framework for possibly reconciling experimental measurements of multiple neural attributes; recent theoretical studies have shown that the network components can interact nonlinearly with surprising results (Marder and Goaillard, 2006; Mejias and Longtin, 2014; Hunsberger et al, 2014) (see Discussion section). The results of our study clearly show how multiple components effect the firing rate variability and might apply to experiments that measure the heterogeneity of these (or possibly other) neural attributes.

The network we consider is noisy with variable spiking similar to that of real cortical neurons, and is excitable (i.e., neurons only fire with noise and/or synaptic coupling). We analyze how intrinsic and network heterogeneity together alter the dynamics of strongly coupled networks of neurons in various regimes ranging from asynchronous to rhythmic (i.e, 'ping' network) firing. We focus on the dynamics of the excitatory neurons because they are the predominate cells for propagating signals to different layers in the cortex. Unsurprisingly, we find that when both intrinsic and network heterogeneity increase independently (i.e., when there is no relationship between them), the excitatory firing rates tend to have a larger range. However, for a fixed level of heterogeneity, the relationship or correlation between intrinsic and network heterogeneity strongly affects the overall range of excitatory firing rates. Moreover, these effects depend on what regime the neural network is in: during rhythmic firing, excitatory firing rate ranges decrease when intrinsic and network heterogeneity correlation increases; during asynchronous firing, excitatory firing rate ranges increase when intrinsic and network heterogeneity correlation increases.

To better understand these observations, we implement a dimension reduction method that relies on a combination of Monte Carlo simulations and analytic reductions. The reduction theory is based in part on our previous work (Ly, 2013; Nicola et al, 2015), and on the work of others (Moreno-Bote and Parga, 2006; Nesse et al, 2008), where particular state variables are assumed to be slow and thus decoupled from other variables. Fortunately, the dimension reduction method captures the qualitative trend of the range of excitatory firing rates as heterogeneity is changed. This further inspires a simpler yet more revealing analytic description for how intrinsic and network heterogeneity combine to yield different ranges of excitatory firing rates. This study gives a more complete understanding of how heterogeneities interact and result in modulation of the firing rate statistics, which may ultimately lead to a better understanding of neural coding in coupled neural networks.

2 Methods

2.1 Recurrent spiking LIF network

The recurrent spiking network of excitatory (E) and inhibitory (I) neurons are modeled as leaky integrate-and-fire (LIF) neurons. The intrinsic and network heterogeneity are modeled simply by two parameters that are allowed to vary among the neurons. Other modeling studies impose heterogeneity in the response property (Tripathy et al, 2013), e.g., orientation tuning (Shamir and Sompolinsky, 2006; Chelaru and Dragoi, 2008). The models here effectively have heterogeneous response properties, but our focus is on two different sources that lead to that property. We model the intrinsic heterogeneity by having different voltage thresholds for spiking (Mejias and Longtin, 2012; Yim et al, 2013), equivalent to how many have incorporated intrinsic heterogeneity (Strogatz and Mirollo, 1991; Chow, 1998; Burton et al, 2012; Ly et al, 2012). The network heterogeneity is modeled by scaling the synaptic input by a value, effectively making each neuron receive different levels of network input. There is evidence in slice recordings that the probability of connection depends on distance (Oswald et al, 2009; Levy and Reyes, 2012), although we are not taking into account spatial dynamics, this model is plausible assuming synaptic strengths do not all inversely scale with connection probability. Moreover, there is abundant evidence for differences in synaptic coupling between neurons (Parker, 2003; Marder and Goaillard, 2006; Bremaud et al, 2007).

The equations for the excitatory neurons indexed by $j \in \{1, 2, \ldots, N_e\}$ are:

$$
\begin{aligned}
\tau_m \frac{dv_j}{dt} &= -v_j - g_{ie}(t)(v_j - \mathcal{E}_I) - g_{ee}(t)(v_j - \mathcal{E}_E) + \sigma_E \eta_j(t) \\
v_j(t^*) &\geq \theta_j (\text{refractory period}) \Rightarrow v_j(t^* + \tau_{ref}) = 0 \\
\tau_n \frac{d\eta_j}{dt} &= -\eta_j + \sqrt{\tau_n}\xi_j(t) \\
g_{ee}(t) &= q_j \frac{\gamma_{ee}}{p_{ee} N_e} \sum_{j' \in \{\text{presyn E cells}\}} G_{j'}(t) \\
g_{ei}(t) &= \frac{\gamma_{ei}}{p_{ei} N_i} \sum_{k' \in \{\text{presyn I cells}\}} G_{k'}(t) \\
\tau_d \frac{dG_j}{dt} &= -G_j + A_j \\
\tau_r \frac{dA_j}{dt} &= -A_j + \tau_r \alpha \sum_l \delta(t - t_l)
\end{aligned}
\tag{1}
$$

where the leak, inhibitory and excitatory reversal potentials are 0, $\mathcal{E}_I$, and $\mathcal{E}_E$, respectively with $\mathcal{E}_I < 0 < \mathcal{E}_E$ (the voltage is scaled to be dimensionless so that a leak/resting value of -65 mV maps to 0 and a threshold voltage of -55 mV maps to 1 (see Table 1)). $\xi_j(t)$ are uncorrelated white noise processes, p_{xy} is the proportion of neuron type y (randomly chosen) that provides presynaptic input to neuron type x ($x, y \in \{e, i\}$). The second line in the equations describes the refractory period at spike time t^*: when the neuron's voltage crosses threshold θ_j (**intrinsic heterogeneity**), the neuron goes into a refractory period for τ_{ref} where the voltage is undefined[1], after which we set the neuron's voltage to 0. In the last line, t_l denotes the spike times of the jth excitatory neuron. There are two factors in the equation for the total synaptic conductances (g_{ee} and g_{ei}): q_j and $\frac{\gamma_{xy}}{p_{xy} N_y}$; the latter does not depend on the individual neuron and is the same across the entire (E) population. However, q_j introduces **network heterogeneity** by scaling *both* excitatory and inhibitory synaptic inputs. This form of network heterogeneity is loosely motivated by recent results by Xue et al (2014), who found that pyramidal neurons receive relatively similar proportions of excitation and inhibition in layer 2/3 of mammalian visual cortex (i.e., some cells receive more E/I while some cells receive less E/I). The q_j factors are a

[1] In refractory, the other variables are governed by their ODEs

Table 1 Parameters for all simulations

Parameter	τ_m	τ_{ref}	$\mathcal{E}_I$	$\mathcal{E}_E$	τ_n	p_{xy}
For E and I:	20 ms	2 ms	-0.5	6.5	5 ms	0.2

Parameter	τ_d	τ_r	α	$N_{e/i}$
E cells	1 ms	5 ms	1	800
I cells	2 ms	10 ms	2	200

Table 2 Parameters for specific regimes

Regime:	γ_{ei}	γ_{ie}	γ_{ee}	γ_{ii}	σ_E	σ_I
Noisy Rhythm	10	8	12.25	5	2.5	3
Asynchronous	10	8	0.05	5	3.5	4
Sharp Rhythm	10	8	11.5	5	2.55	–

straight forward way to capture the different levels of 'balanced' input (see equation (2)). The term network heterogeneity is often used to mean that the structure of the network is heterogeneous; here, we use that term to mean that the network activity induces heterogeneity via network inputs.

Similarly, for the inhibitory neurons indexed by $k \in \{1, 2, \ldots, N_i\}$, the equations are:

$$\begin{aligned}
\tau_m \frac{dv_k}{dt} &= -v_k - g_{ii}(t)(v_k - \mathcal{E}_I) - g_{ei}(t)(v_k - \mathcal{E}_E) + \sigma_I \eta_k(t) \\
v_k(t^*) &\geq 1 (\text{refractory period}) \Rightarrow v_j(t^* + \tau_{ref}) = 0 \\
\tau_n \frac{d\eta_k}{dt} &= -\eta_k + \sqrt{\tau_n}\xi_k(t) \\
g_{ie}(t) &= q_j \frac{\gamma_{ie}}{p_{ie} N_e} \sum_{k' \in \{\text{presyn I cells}\}} G_{k'}(t) \\
g_{ii}(t) &= \frac{\gamma_{ii}}{p_{ii} N_i} \sum_{k' \in \{\text{presyn I cells}\}} G_{k'}(t) \\
\tau_d \frac{dG_k}{dt} &= -G_k + A_k \\
\tau_r \frac{dA_k}{dt} &= -A_k + \tau_r \alpha \sum_l \delta(t - t_l)
\end{aligned} \tag{2}$$

Notable differences compared to excitatory neurons are that the threshold values are all equal to 1, and there is not a q_k factor that scales the presynaptic inputs from the network. Although one could in principle relax these assumptions and augment the subsequent theory in a standard way, we made this choice because the results in this paper would not be diminished, and to avoid distracting from our focus on excitatory neuron behavior. The parameter values for all of the figures are in Table 1.

We consider two regimes of this model: (i) **noisy rhythm**, where the power spectrum is larger for certain frequency values, and (ii) **asynchronous** that has a flat power spectrum. Figure 1 shows a comparison of various quantities in the three regimes considered in this paper (see Table 2 for parameter values of different regimes).

Monte Carlo Simulations: Monte Carlo simulations were run for 100 s of simulation time for ten realizations (Fig. 1 has only one realization) with a time step $\Delta t = 0.2$ ms, and the firing rates statistics were binned in non-overlapping 1 ms time windows. We use a common estimate of the standard deviation of

the firing rate calculations with Monte Carlo simulations across the $n = 10$ realizations:

$$\overline{\sigma_{\nu(j)}} \approx \sqrt{\frac{1}{n-1}\sum_{m=1}^{n}\left(\nu_m(j) - \overline{\nu_m(j)}\right)^2};$$

the gray shaded regions in panels A and C of Figures 2–4 represent 1 standard deviation above and below the sample mean: $\overline{\nu_m(j)} \pm \overline{\sigma_{\nu(j)}}$. The Monte Carlo simulation plots in panel B of Figures 2–4 did not include standard deviation regions because the plots would be harder to see. The error bars of the Monte Carlo simulations in panel D of Figures 2–4 and Figure 5A, C, E, represent an estimate of the standard deviation of: $\max_j \nu - \min_j \nu$. We use the following estimate:

$$\overline{\sigma_{\nu(\max)-\nu(\min)}} \approx \sqrt{\overline{\sigma_{\nu(\max)}}^2 + \overline{\sigma_{\nu(\min)}}^2}$$

even though $\overline{\sigma_{\nu(\max)-\nu(\min)}} = \sqrt{\overline{\sigma_{\nu(\max)}}^2 + \overline{\sigma_{\nu(\min)}}^2 - 2Cov(\nu(\max), \nu(\min))}$; the reason for this is because estimating $2Cov(\nu(\max), \nu(\min))$ would require storing an additional $O(N_e^2)$ sized vector, as well as $O(n^2)$ simulations for similar order accuracy (for every single parameter set), and the computation times are already quite long.

2.2 Model with a sharper rhythm

Another model considered is one with less variable inhibitory firing that ultimately leads to sharper rhythms in the excitatory neurons. The reason for an observed sharper rhythm (Fig. 1F) is that in these recurrent networks, the inhibitory neuron firing silence and thus shape the rhythm of the excitatory neurons (Börgers and Kopell, 2003; Economo and White, 2012). The only change is in the inhibitory neuron's voltage equation which no longer has a noise term, but rather a deterministic drift to a subthreshold target voltage $\mathcal{E}_{det}$:

$$\tau_m \frac{dv_k}{dt} = -v_k - g_{ii}(t)(v_k - \mathcal{E}_I) - g_{ie}(t)(v_k - \mathcal{E}_E) - g_{det}(v_k - \mathcal{E}_{det})$$

we set $\mathcal{E}_{det} = 0.9$ and $g_{det} = 2$. The regime considered has a strong and relatively regular oscillation (Figure 1 right column **sharp rhythm**).

In addition to showing distinct characteristics compared to the other regimes (noisy rhythm, asynchronous), the main motivation for considering this additional model is that such recurrent networks with a sharp gamma rhythm are commonly studied and known to be important for coding in many areas of the cortex (Börgers and Kopell, 2003; Wang, 2010; Buzsáki and Wang, 2012; Economo and White, 2012).

The following two subsections describe the way both network and intrinsic heterogeneity are modulated in this paper.

2.3 Changing the level of intrinsic and network heterogeneity independently

The two heterogeneous parameters (q_j, θ_j) are varied to yield significant changes in the range of firing rates. The means of both $\mathbf{q}$ and $\boldsymbol{\theta}$ are set to 1, and the parameters $\sigma_q \in [0, 1]$ and $\sigma_\theta \in [0, 1]$ quantify the level of the network and intrinsic heterogeneities, respectively, in the following way:

$$\mathbf{q} \sim 1 + \sigma_q * (\mathcal{U} - 0.5) \tag{3}$$

$$\boldsymbol{\theta} \sim 1 + \sigma_\theta * \mathcal{N} \tag{4}$$

where $\mathcal{U}$ is the uniform distribution on $[0, 1]$, and $\mathcal{N}$ is a truncated[2] normal distribution with mean 0 and standard deviation 0.08. When chosen independently, the correlation between these two vectors will be small and theoretically zero.

2.4 Changing the correlation between intrinsic and network heterogeneity

We consider another way to change the heterogeneity where the overall level is approximately the same but the correlation between $\mathbf{q}$ and $\boldsymbol{\theta}$ is set to a prescribed value. Given the vectors $\mathbf{q}$ and $\boldsymbol{\theta}$, we fix $\mathbf{q}$ to the same values but transform $\boldsymbol{\theta}$ so that the Pearson's correlation coefficient is $\varrho \in (-1, 1)$ in such a way that the transformed vector has the same mean and variance as $\boldsymbol{\theta}$. The details for how this is accomplished are described in the Appendix.

2.5 High dimensional probability density equation

The recurrent coupled stochastic network in section 2.1 is difficult to describe theoretically. A common method uses probability density functions (p.d.f.), or a population density methods, where the probability of a neuron being in a particular state has a corresponding equation. The variables in the populations are no longer tracked individually, but rather captured by a p.d.f.; for example, (V_j, G_j, A_j, η_j) for $j = 1, 2, \ldots, N_e$ are captured with a function of (v_E, g_E, a_E, η_E). The two forms of heterogeneity introduce even more dimensions than the usual state variables. For simplicity, one can track a family of probability density functions for each (q_j, θ_j) pair or each distinct neuron. The subsequent equations are a good approximation to the coupled network (1)-(2) with the following assumptions:

(i) finite size effects are negligible ($N_{e/i} \gg 1$)
(ii) the firing rate of presynaptic neurons is governed by a Poisson process
(iii) the population firing rate averaged over $\mathbf{q}$ and $\boldsymbol{\theta}$ is a good approximation to the average presynaptic input rate
(iv) a single p.d.f. function is adequate to describe the population behavior, and the heterogeneity is driven by (q_j, θ_j)

The first two assumptions are standard in this framework, while the last two assumptions has been successfully used (Ly, 2014), where a family of probability density functions were indexed by the quenched heterogeneity values. Even though these assumptions are violated, the following equations are key for the reduced descriptions in sections 2.6, 3.2–3.3.

For each pair of values (q_j, θ_j), the probability density function ρ is defined by:

$$\int_{\Omega} \rho(v_E, \mathbf{w}_E, v_I, \mathbf{w}_I, t)\, dv_E\, d\mathbf{w}_E\, dv_I d\mathbf{w}_I = \Pr\Big(\big(v_E(t), \mathbf{w}_E(t), v_I(t), \mathbf{w}_I(t)\big) \in \Omega\Big)$$

where $\mathbf{w}_X$ denotes the other states variables of the corresponding neuron type $X \in \{E, I\}$, consisting of conductance, colored noise: $\mathbf{w}_X = (g_X, a_X, \eta_X)$. The evolution of the p.d.f.'s is governed by a continuity equation and boundary conditions:

[2] The middle 98.76% is included, so for $\sigma_\theta = 1$, $\boldsymbol{\theta} \in [0.8, 1.2]$

$$
\begin{aligned}
\frac{\partial \rho}{\partial t} &= -\nabla \cdot \mathbf{J} && (5)\\
\mathbf{J} &:= (J_{v_E}, J_{g_E}, J_{a_E}, J_{\eta_E}, J_{v_I}, J_{g_I}, J_{a_I}, J_{\eta_I}) && (6)\\
J_{v_E} &:= -\frac{1}{\tau_m}\left[v_E + q\gamma_{ei} g_I (v_E - \mathcal{E}_I) + q\gamma_{ee} g_E (v_E - \mathcal{E}_E) + \sigma_E \eta_E\right]\rho && (7)\\
J_{v_I} &:= -\frac{1}{\tau_m}\left[v_I + \gamma_{ii} g_I (v_I - \mathcal{E}_I) + \gamma_{ie} g_E (v_I - \mathcal{E}_E) + \sigma_I \eta_I\right]\rho && (8)\\
J_{g_X} &:= -\frac{1}{\tau_d}\left[g_X - a_X\right]\rho && (9)\\
J_{a_X} &:= -\frac{a_X}{\tau_r} + \nu_X(t)\int_{a_X-\alpha_X}^{a_X} \rho(\dots, a'_X, \dots)\, da'_X && (10)\\
J_{\eta_X} &:= -\frac{1}{\tau_n}\eta_X \rho + \frac{1}{\tau_n}\frac{\partial^2 \rho}{\partial \eta_X^2} && (11)\\
\nu_X(t) &:= \frac{1}{\tau_m}\int\int\int J_{v_X}(v_X = \theta, \mathbf{w}_X)\, d\mathbf{w}_X\, dq\, d\theta && (12)\\
J_{v_X}(v_X = \theta, \mathbf{w}_X, t) &= J_{v_X}(v_X = 0, \mathbf{w}_X, t + \tau_{ref}) && (13)\\
J_{\mathbf{w}_X}|_{\partial \mathbf{w}_X} &= 0 && (14)
\end{aligned}
$$

The definitions of g_{XY} in the LIF equations (1)-(2) result in a total conductance of $\gamma_{XY} g_Y$ on average. Note that with a refractory period $\tau_{ref} > 0$, the system of equations should also include a refractory probability density that we do not state here (see the work of Tranchina and colleagues Nykamp and Tranchina (2001); Haskell et al (2001); Apfaltrer et al (2006); Ly and Tranchina (2009) for further details).

2.6 Reduction theory to describe firing rate dynamics

We describe an insightful analytic reduction that captures how the range of excitatory firing rates change in different regimes. We focus on only the excitatory neurons, which have fewer state variables if the inhibitory population is ignored or assumed to be known. The problem with using the full p.d.f equations (5)–(14) is that the state variables are coupled, so we will formally assume that all of the state variables are known (given) except v_E, and solve for the steady-state firing rate as a function of the other state variables (Ly, 2013; Nicola et al, 2015). Note that other authors have employed a similar approach using an adiabatic or slow variable approximation in the context of stochastic spiking neurons (Moreno-Bote and Parga, 2006; Nesse et al, 2008); very recently Hertäg et al (2014) used this approach formally (see their equation (25)).

We denote r as the approximation to the excitatory firing rate(s) ν_E. Assuming the other state variables are simply parameters, the deterministic firing rate of the equation

$$
\tau_m \frac{dv_E}{dt} = -v_E - q\tilde{g_I}(v_E - \mathcal{E}_I) - q\tilde{g_E}(v_E - \mathcal{E}_E) + \tilde{\eta_E}
$$

is straightforward to calculate, and given by

$$
r_0(q, \theta; \tilde{\mathbf{w}_E}) = \begin{cases} 0, & \text{if } \frac{q(\tilde{g_E}\mathcal{E}_E + \tilde{g_I}\mathcal{E}_I) + \tilde{\eta_E}}{1 + q(\tilde{g_E} + \tilde{g_I})} \le \theta \\ \frac{1 + q(\tilde{g_E} + \tilde{g_I})}{\tau_m \log\left(\frac{q(\tilde{g_E}\mathcal{E}_E + \tilde{g_I}\mathcal{E}_I) + \tilde{\eta_E}}{q(\tilde{g_E}\mathcal{E}_E + \tilde{g_I}\mathcal{E}_I) + \tilde{\eta_E} - \theta(1 + q(\tilde{g_E} + \tilde{g_I}))}\right)}, & \text{if } \frac{q(\tilde{g_E}\mathcal{E}_E + \tilde{g_I}\mathcal{E}_I) + \tilde{\eta_E}}{1 + q(\tilde{g_E} + \tilde{g_I})} > \theta \end{cases} \quad (15)
$$

The argument of the left-hand side is written in this way because **we assume the q and θ values are the primary sources of heterogeneity**, rather than the external noise, finite size effects, random connectivity, etc. For exposition, we have absorbed the parameters and defined new variables with tildes:

$\tilde{g_E} = \gamma_{ee} g_E$, $\tilde{g_I} = \gamma_{ei} g_I$, $\tilde{\eta_E} = \sigma_E \eta_E$. The approximation (15) ignores the refractory period, which is accounted for via a transformation rather than using the refractory probability density. The inverse of the firing rate is the time between spikes, so the refractory period can be added to the time between spikes to yield: $r_0/(1 + \tau_{ref} r_0)$ as a simple approximation to the firing rate. Finally, the given state variables are integrated against their marginal density to get:

$$r(q, \theta) = \mathbb{E}\left[\frac{r_0}{1 + r_0 \tau_{ref}}\right] = \int \frac{r_0}{1 + r_0 \tau_{ref}} \tilde{\rho}(\tilde{g_E}, \tilde{g_I}, \tilde{\eta_E})\, d\tilde{\mathbf{w}}_E \tag{16}$$

There is a slight abuse of notation because the auxiliary variables a_X effect the conductances but are not written in the previous equation; the emphasis is on how $(\tilde{g_E}, \tilde{g_I}, \tilde{\eta_E})$ directly effects r. Since the external noise is applied indiscriminately, $\tilde{\eta_E}$ is independent of the other variables and the marginal density factors into:

$$\tilde{\rho}(\tilde{g_E}, \tilde{g_I}, \tilde{\eta_E}) = \tilde{\rho}(\tilde{g_E}, \tilde{g_I}) \frac{e^{-(\tilde{\eta_E}/\sigma_E)^2}}{\sigma_E \sqrt{\pi}}.$$

However, $\tilde{\rho}(\tilde{g_E}, \tilde{g_I})$ is still not analytically tractable, leading us to rely on Monte Carlo simulations to numerically estimate $\tilde{\rho}(\tilde{g_E}, \tilde{g_I})$.

The reduction method (15)–(16) was implemented by relying on Monte Carlo simulations for $\tilde{\rho}(\tilde{g_E}, \tilde{g_I})$, and using the same vectors $(\mathbf{q}, \boldsymbol{\theta})$ in the LIF simulations. Since $\tilde{\rho}(\tilde{g_E}, \tilde{g_I})$ is the same for a given parameter set, the range of firing rates is theoretically captured by the different (q_j, θ_j) values in equation (16) (see blue curves in Figs. 2–4).

3 Results

We consider a recurrently coupled stochastic spiking neural network. Such networks have been ubiquitous in contemporary theoretical investigations. The class of networks considered here are widely used even though we do not include plasticity or detailed biophysical properties with different time scales. We are interested in how the firing rate of the excitatory population changes as the level of heterogeneity is varied in different regimes. Excitatory neurons are the focus because they are the predominate cells for propagating signals to different layers in the cortex.

Figure 1 highlights the different behaviors in three regimes considered. Representative raster plots of spikes are shown in panels A–C for both excitatory and inhibitory cells, incorporating both forms of heterogeneity with $(\mathbf{q}, \boldsymbol{\theta})$ chosen independently and with $\sigma_q = \sigma_\theta = 1$. In panels D–F, the power spectrum of the excitatory population firing rate for both heterogeneous (black) and homogeneous parameters (magenta) are shown; the thinner lines are the power spectrums of the individual excitatory neurons. The inset shows the autocorrelation function of the (E) population firing rate. The autocorrelation function of a stochastic process $R(t)$ (e.g., excitatory population firing rate) is:

$$A(t) = \mathbb{E}_\tau\left[R(\tau)R(t-\tau)\right] - \mathbb{E}_\tau[R(\tau)]^2 \tag{17}$$

and the power spectrum is:

$$P(\omega) = \left| \int A(t) e^{-i2\pi\omega t}\, dt \right|. \tag{18}$$

These quantities illustrate the different dynamics of each neural network. Notice that the power spectrum of the individual neurons is consistently larger in value than the power spectrum of the population firing rate. This is because the population firing rate is averaged (smoothed) so that $P(\omega) \to 0$ for large frequencies, whereas the spike train of the individual neurons is not smooth, consisting of 0's or $\delta's \approx 1/(\Delta t)$ that will always yield $P_j > 0$ as long as $\omega < 1/(\Delta t)$ (the numerical limit because of the discretization). Specifically, as $\omega \to 1/(\Delta t)$, P_j measures the average power of the spike train in a single time bin and thus converges to the firing rate of the individual neuron. The bottom row (panels G–I) show the distribution of the excitatory firing rates for each individual neuron, averaged

Table 3 Firing Rate Values in Figure 1 G–I. The inhibitory firing rates are not shown in Figure 1.

Regime:	Mean ν (Hz)	$[\nu_{min}, \nu_{max}]$ (Hz)	Range of ν (Hz)
Noisy Rhythm (Heterog.): E cells	12.8	[6.6, 23]	16.4
Noisy Rhythm (Homog.): E cells	11.6	[10.3, 12.7]	2.5
Asynchronous (Heterog.): E cells	7.7	[2.7, 14.2]	11.4
Asynchronous (Homog.): E cells	7.4	[6.5, 8.2]	1.7
Sharp Rhythm (Heterog.): E cells	34.1	[14.2, 64]	49.8
Sharp Rhythm (Homog.): E cells	33.6	[32.1, 35.5]	3.5
Noisy Rhythm (Heterog.): I cells	17	[15.9, 18.7]	2.8
Noisy Rhythm (Homog.): I cells	16.1	[14.8, 17.4]	2.6
Asynchronous (Heterog.): I cells	19.7	[18.5, 21.2]	2.7
Asynchronous : Homog. I cells	19.6	[17.9, 20.9]	3
Sharp Rhythm (Heterog.): I cells	26.8	[17.4, 32.4]	15
Sharp Rhythm (Homog.): I cells	26	[24.3, 27.9]	3.6

over time (simulations in Figure 1 were performed for 100 s). The heterogeneous population naturally has a wider distribution compared to the homogeneous regime. At the population level, there are only minor differences between the homogeneous and heterogeneous regimes; indeed, the average firing rates (not the overall distribution), power spectrums, and autocorrelation functions are very similar. Thus enabling a systematic assessment of how intrinsic and network heterogeneity effect the spiking network, avoiding the complication of regime changes due to heterogeneity. Although there has been interesting work showing how heterogeneity can induce rhythms from asynchrony (i.e., bifurcations) (Hermann and Touboul, 2012; Mejias and Longtin, 2012), we do not directly address such dynamics here. Our study focuses on comparing the firing rate heterogeneity modulation *within* specific regimes.

The neurons in all regimes considered are all excitable and receive external colored noise, resulting in irregular spiking. A common measure of variability is the Fano factor, defined as the variance of spike counts divided by the mean of spike counts in a time window. For all of the networks considered in this paper (e.g., Fig. 1), the Fano factor of the E population spike counts is often greater than 1 and is at least 0.8 for heterogeneous and homogeneous networks, across all regimes, and for time windows ranging from 2 to 50 ms (not shown).

3.1 PDF framework captures firing rate modulation with heterogeneity

The level of intrinsic and network heterogeneity were modulated in the recurrently coupled networks in the two ways previously described: i) independently choose the vectors $(\mathbf{q}, \boldsymbol{\theta})$ with a prescribed level of heterogeneity determined by σ_q and σ_θ (see (3)–(4)), and ii) for fixed values of $\sigma_{q/\theta}$, change the correlation between $(\mathbf{q}, \boldsymbol{\theta})$. In the noisy rhythm regime, Figure 2A shows the minimum and maximum excitatory firing rates for fixed values of $\sigma_q = 0$ and 1, while σ_θ varies between 0 and 1 (black curves; dashed and solid). Not surprisingly, as σ_θ (or σ_q) increased, so does the range of (excitatory) firing rates with the minimum decreasing and maximum increasing. Note that we chose to plot the curves for fixed σ_q; the results also hold with fixed σ_θ and σ_q on the x-axis (not shown). Figure 2B shows the range of the firing rates (maximum minus the minimum) rather than the raw firing rate values; it is apparent that more intrinsic and/or network heterogeneity leads to more firing rate heterogeneity. The reduction theory described in section 2.6 (based on both probability density equations and Monte Carlo simulations), and in particular equations (15)–(16) for the approximation of the firing rates, are shown in the blue colored curves. In Figure 2A, the theory does not provide a good quantitative match. This could be due to a variety of reasons: the 4 assumptions in section 2.5 are violated, the reduction method is known to be inaccurate compared to both the full PDF and Monte Carlo simulations. Fortunately, the reduction theory is able to capture the increase in the firing rate range in Figure 2B, where $\sigma_{q,\theta} \in [0, 1]$. This result is indeed fortuitous given the inaccuracies of the PDF theory in capturing the raw firing rates.

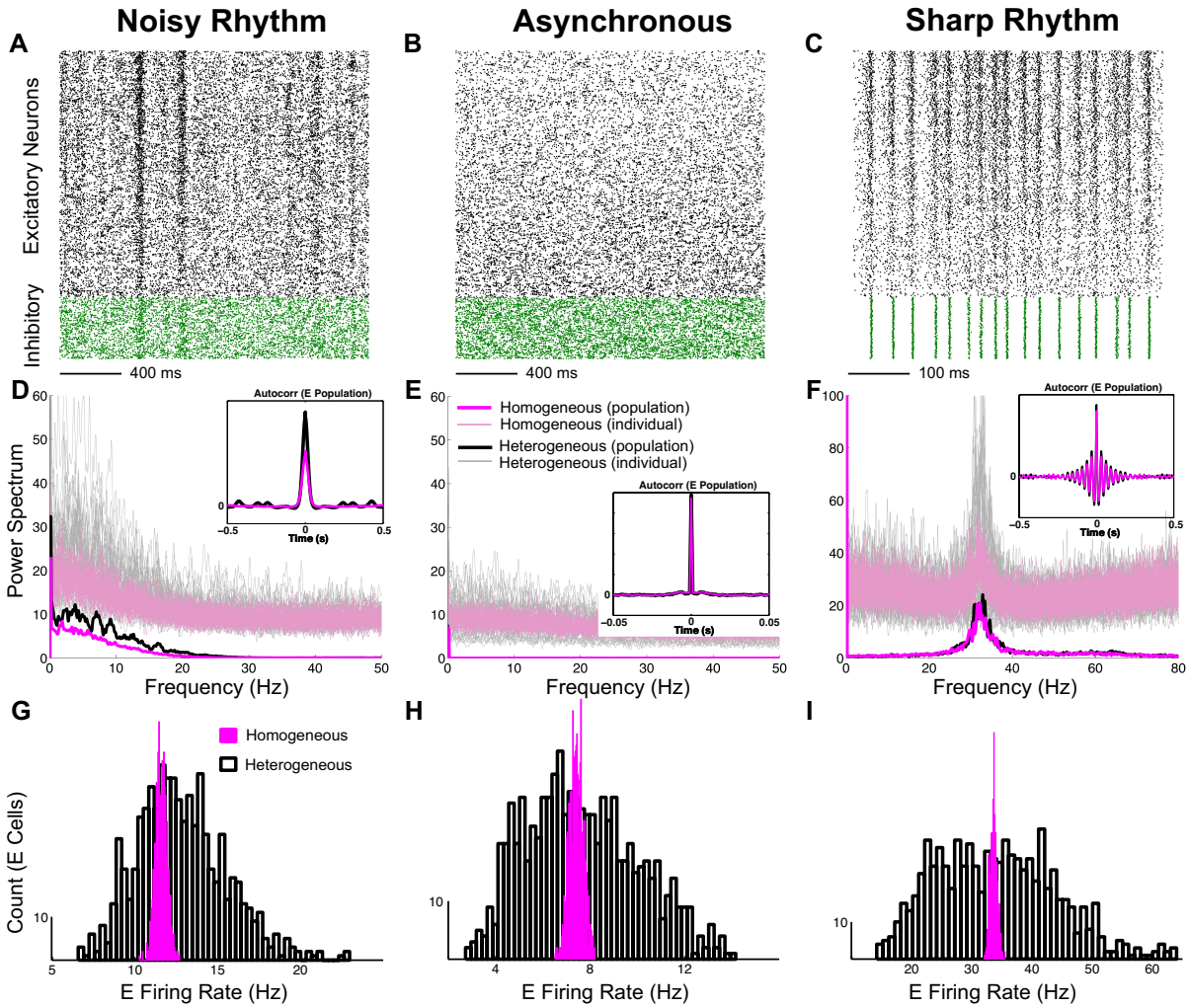

Fig. 1 The three regimes considered are: noisy rhythm (left column, A, D, G), asynchronous (middle column, B, E, H), sharp rhythm (right column, C, F, I). The top row (A–C) has representative raster plots of spikes for both excitatory (black dots) and inhibitory (green dots) neurons with both intrinsic and network heterogeneity, showing distinct behavior depending on the regime. The middle row (D–F) shows the power spectrum of the excitatory population firing rate with both forms of heterogeneity (black) and homogeneous parameters (magenta); the power spectrum of the individual excitatory neurons are shown with thinner lines. The inset of each panel shows the autocorrelation function of the excitatory population rate. The bottom row (G–I) has histograms of the average firing rate for each excitatory neuron, with the heterogeneous network naturally having a wider distribution. The mean firing rate, minimum and maximum firing rates, and the range of the firing rates are displayed in Table 3. The intrinsic and network heterogeneity parameters were selected independently with $\sigma_q = \sigma_\theta = 1$ (see (3)–(4)). The simulations were performed for a single realization of 100 s.

Figure 2C shows the minimum and maximum firing rate with ample heterogeneity ($\sigma_q = \sigma_\theta = 1$, the most we considered), but the correlation between $\mathbf{q}$ and $\boldsymbol{\theta}$ ($\varrho(\mathbf{q}, \boldsymbol{\theta})$) varied between (-1,1). The comparison of the reduction theory (15)–(16) (blue curves) and the simulations (black curves) is not accurate (as in Fig. 2A), but does qualitatively capture the trend in the range of the firing rates (Fig. 2D). The range of firing rates tends to decrease as $\varrho(\mathbf{q}, \boldsymbol{\theta})$ increases. Note that the range of firing rates can be very large and very small depending on ϱ, even though $\sigma_q = \sigma_\theta = 1$; in fact, the ranges of firing rates are comparable to varying the overall level of heterogeneity: $\sigma_{q/\theta} \in [0, 1]$ (Fig. 2A–B). In other words, a particular range of excitatory firing rates can arise from different levels of intrinsic and network heterogeneity, *depending on their relationship*.

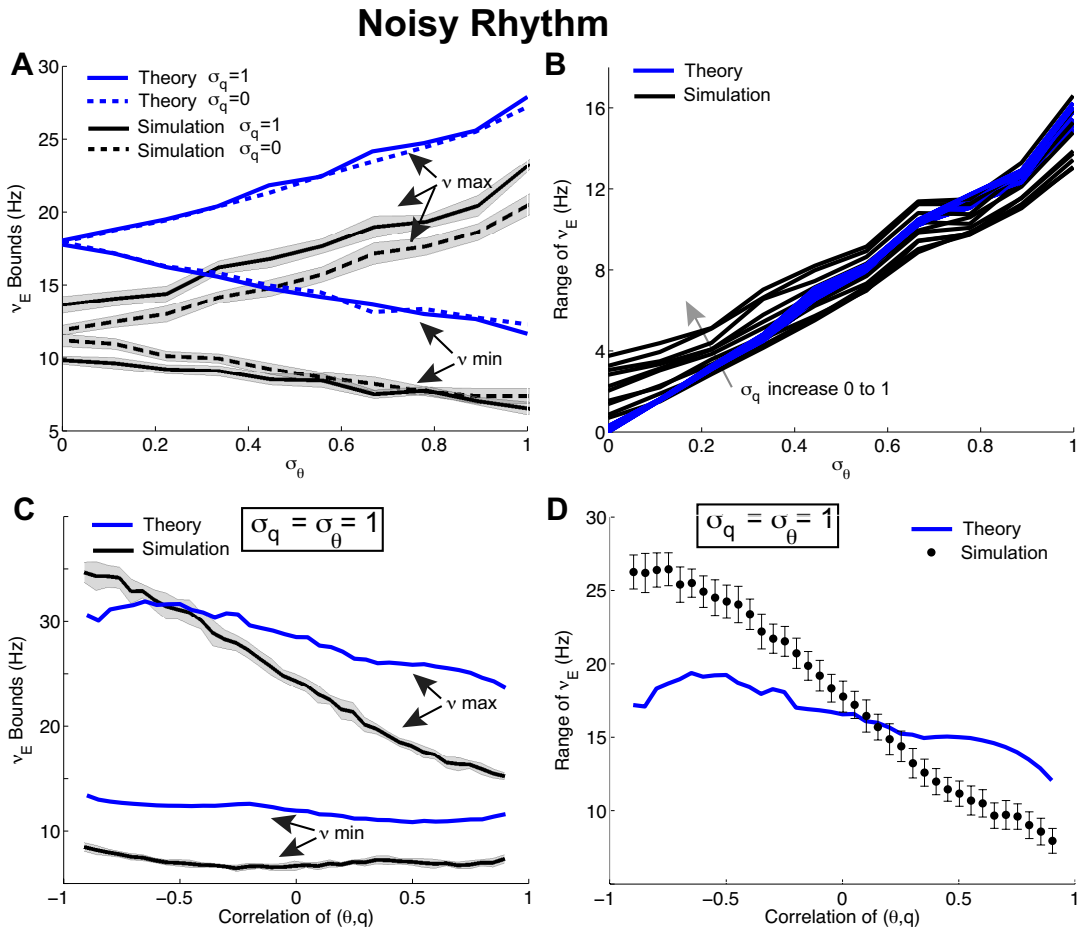

Fig. 2 Noisy Rhythm regime: excitatory firing rates modulation with changes in intrinsic and network heterogeneity. A)–B) changing the level of intrinsic σ_θ and network σ_q heterogeneity by independently drawing $(\mathbf{q}, \boldsymbol{\theta})$ (see (3)–(4)). A) The minimum and maximum firing rates are shown for the homogeneous network ($\sigma_q = \sigma_\theta = 0$, dash curves) and completely heterogeneous ($\sigma_q = \sigma_\theta = 1$, solid curves) network. The simulation curves (black curves, dash and solid) are Monte Carlo simulations of equations (1)–(2) (shaded regions denote standard deviations). Here, the **theory** uses a combination of dimensionally reduced PDF functions and Monte Carlo simulations (see (15)–(16)). Although the theory does not quantitatively match the extreme values of the firing rates (A), it captures the trend of the firing rate range (maximum minus minimum) in panel B); there, each curve is for a fixed value of σ_q ranging from 0 to 1, as σ_θ ranges between 0 and 1. Unsurprisingly, as heterogeneity increases so does the firing rate range. The firing rates and the range vary appreciably over an order of magnitude. C)–D) changing the correlation ϱ between $(\mathbf{q}, \boldsymbol{\theta})$ with $\sigma_q = \sigma_\theta = 1$. C) the theory (blue curve) does not quantitatively capture the actual firing rates as ϱ varies between (-1,1), but they are comparable. D) the theory (solid) captures the trend in the simulated range of the firing rates (dots) as ϱ varies between (-1,1). As ϱ increases, the range of firing rates tends to decrease. Gray shaded regions in A and C are an estimate of the standard deviation about the sample mean of the Monte Carlo simulations (100 s simulation for each realization, 10 realizations total); error bars in D are estimates of the standard deviation about the sample mean of the range (see last paragraph of Section 2.1 for details). Shaded regions are omitted in B for readability.

Similar comparisons are made for the two other regimes in Figures 3 and 4. In the asynchronous regime, as the the heterogeneity parameters are selected independently (Fig. 3A–B), we again see that more heterogeneity leads to a wider range of firing rates. Figure 3A shows $\sigma_q = 0$ and 1 split into two panels so it is easier to compare the theory (15)–(16) and simulations (1)–(2). The quantitative match is not good (Fig. 3A) as expected given the previous figure, but the trend is captured (Fig. 3B, where $\sigma_{q,\theta} \in [0, 1]$). For the bottom row, we fix $\sigma_q = \sigma_\theta = 1$ and let the correlation ϱ between intrinsic and network heterogeneity vary between (-1,1). Notice that the range of firing rates changes in a different way

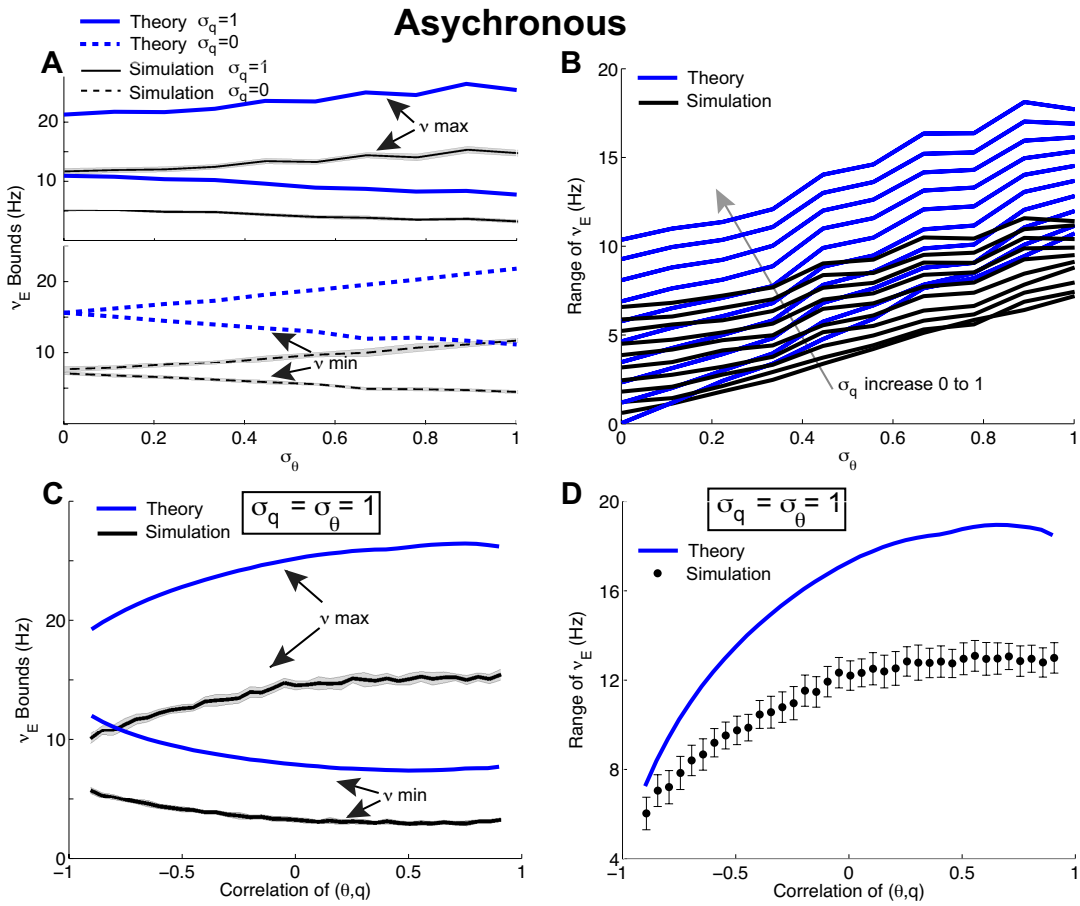

Fig. 3 Asynchronous regime: excitatory firing rates modulation with changes in intrinsic and network heterogeneity [similar to Figure 2] A)–B) changing the level of intrinsic σ_θ and network σ_q heterogeneity by independently drawing $(\mathbf{q}, \boldsymbol{\theta})$ (see (3)–(4)). A) The minimum and maximum firing rates are shown for the completely heterogeneous ($\sigma_q = \sigma_\theta = 1$, solid curves) network in the top panel and the homogeneous network ($\sigma_q = \sigma_\theta = 0$, dash curves) in the bottom panel. The simulation curves (black curves, dash and solid) are Monte Carlo simulations of equations (1)–(2). Here, the **theory** uses a combination of dimensionally reduced PDF functions and Monte Carlo simulations (see (15)–(16)). Although the theory does not quantitatively match the extreme values of the firing rates (A), it captures the trend of the firing rate range (maximum minus minimum) in panel B); there, each curve is for a fixed value of σ_q ranging from 0 to 1, as σ_θ ranges between 0 and 1. Unsurprisingly, as heterogeneity increases so does the firing rate range. C)–D) changing the correlation ϱ between $(\mathbf{q}, \boldsymbol{\theta})$ with $\sigma_q = \sigma_\theta = 1$. C) the theory (blue curve) does not quantitatively capture the actual firing rates as ϱ varies between (-1,1). D) the theory (solid) captures the trend in the simulated range of the firing rates (dots) as ϱ varies between (-1,1). As ϱ increases, the range of firing rates tends to increase. Gray shaded regions in A and C are an estimate of the standard deviation about the sample mean of the Monte Carlo simulations (100 s simulation for each realization, 10 realizations total); error bars in D are estimates of the standard deviation about the sample mean of the range (see last paragraph of Section 2.1 for details). Shaded regions are omitted in B for readability.

(Fig. 3D). Here, as ϱ increases, the range of firing rates *increases* in contrast to before where it decreased (Fig. 2D). Moreover, we see the range of firing rates change by a factor of $\sim$3, which interestingly is comparable to the firing rate range values when varying $\sigma_{q/\theta}$ independently (Fig. 3A–B).

In Figure 4, the sharp rhythm regime shows similar characteristics to Figure 2, except for the following. The excitatory firing rate range is more sensitive to varying the heterogeneity parameters, and we see that the range of firing rates takes on much larger values. This is apparent both when σ_q and σ_θ vary independently (Fig. 4A–B) and when the correlation between $\mathbf{q}$ and $\boldsymbol{\theta}$ changes with $\sigma_q = \sigma_\theta = 1$ (Fig. 4C–D). The firing rate range changes by almost an order of magnitude. The other interesting thing about this regime is that the reduction theory (blue) matches the simulations much better than

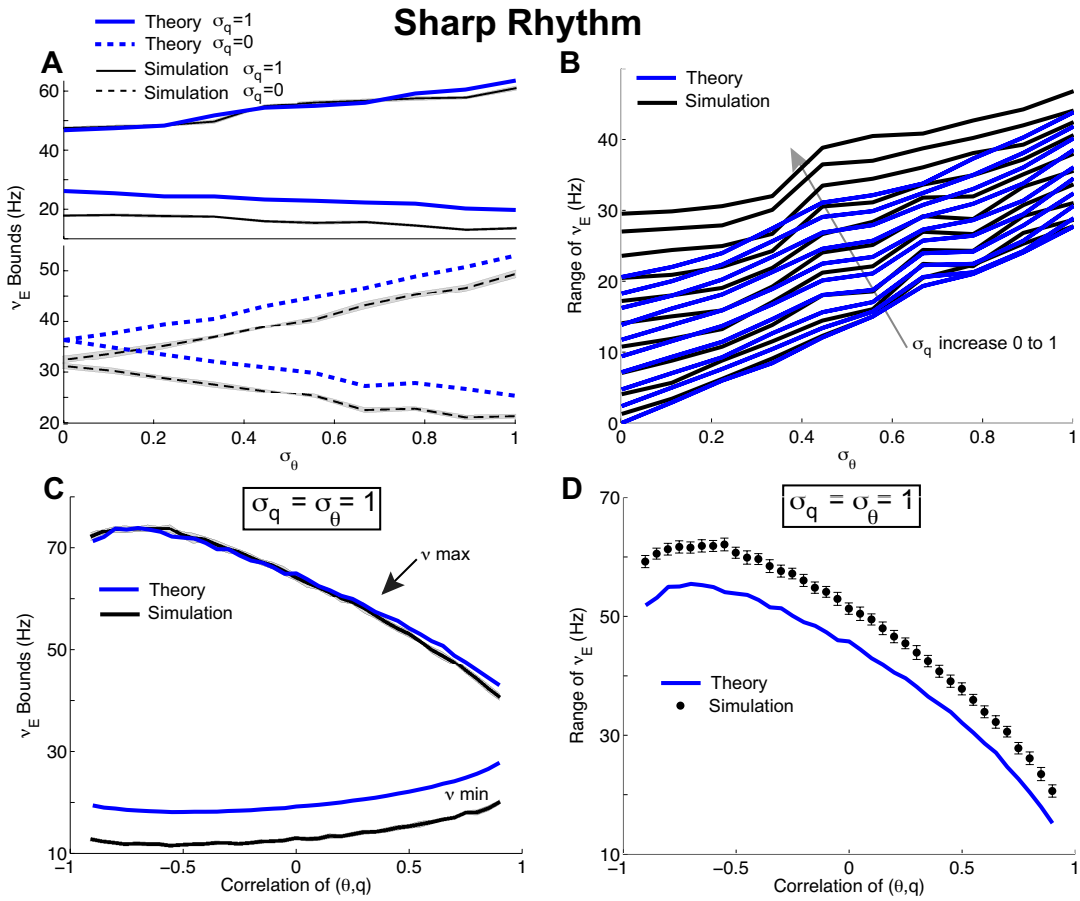

Fig. 4 Sharp Rhythm regime: excitatory firing rates modulation with changes in intrinsic and network heterogeneity [similar to Figures 2–3] A)–B) changing the level of intrinsic σ_θ and network σ_q heterogeneity by independently drawing $(\mathbf{q}, \boldsymbol{\theta})$ (see (3)–(4)). A) The minimum and maximum firing rates are shown for the completely heterogeneous ($\sigma_q = \sigma_\theta = 1$, solid curves) network in the top panel and the homogeneous network ($\sigma_q = \sigma_\theta = 0$, dash curves) in the bottom panel. The simulation curves (black curves, dash and solid) are Monte Carlo simulations of equations (1)–(2). Here, the **theory** uses a combination of dimensionally reduced PDF functions and Monte Carlo simulations (see (15)–(16)). Although the theory does not quantitatively match the extreme values of the firing rates (A), it captures the trend of the firing rate range (maximum minus minimum) in panel B); there, each curve is for a fixed value of σ_q ranging from 0 to 1, as σ_θ ranges between 0 and 1. Unsurprisingly, as heterogeneity increases so does the firing rate range. C)–D) changing the correlation ϱ between $(\mathbf{q}, \boldsymbol{\theta})$ with $\sigma_q = \sigma_\theta = 1$. C) again, the theory (blue curve) does not quantitatively capture the actual firing rates as ϱ varies between (-1,1). D) the theory (solid) captures the trend in the simulated range of the firing rates (dots) as ϱ varies between (-1,1). As ϱ increases, the range of firing rates tends to decrease. Gray shaded regions in A and C are an estimate of the standard deviation about the sample mean of the Monte Carlo simulations (100 s simulation for each realization, 10 realizations total); error bars in D are estimates of the standard deviation about the sample mean of the range (see last paragraph of Section 2.1 for details). Shaded regions are omitted in B for readability.

the other two regimes (Fig. 2–3). The match is particularly good for the maximum firing rate. Similar to the noisy rhythm regime, we see that as ϱ increases, the range of firing rates decreases dramatically (Fig. 4D). One striking observation is that the PDF theory captures the firing rates much better in the sharp rhythm regime (Fig. 4C–D) than the other two regimes (Fig. 2C–D, Fig. 3C–D). Although the underlying reason for this is difficult to determine exactly, a plausible explanation is that the overall higher firing rates and less noise in the sharp rhythm regime are consistent with the assumptions of the approximation in equation (15).

The observation that more intrinsic and (uncorrelated) network heterogeneity leads to a wider range of firing rates (Figs. 2–4, panels A and B) is expected and does not require further analytical insight.

However, changing the correlation between $\mathbf{q}$ and $\boldsymbol{\theta}$ for fixed values of σ_q and σ_θ results in enlarged or diminished ranges of firing rates, depending on the regime (Figs. 2–4, panels C and D). **How can these observations be reconciled?** The next two sections provide further analysis to deeply understand these phenomena.

3.2 Analytic description of heterogeneous firing rate range in rhythmic networks

For many regimes and the different types of heterogeneity, the reduction method in section 2.6 does qualitatively capture the modulation of the range of firing rates, as shown in Figures 2–4, panels B and D. This observation is the motivation for further analysis of equations (15)–(16) that ultimately yields simple analytic formulas to account for how the firing rate ranges are effected by the relationship between intrinsic and networks heterogeneity. In sections 3.2 and 3.3, we use the following variable substitutions to facilitate exposition of the analysis:

$$x_0 := \tilde{g_E} + \tilde{g_I} \tag{19}$$

$$x_1 := \tilde{g_E}\mathcal{E}_E + \tilde{g_I}\mathcal{E}_I \tag{20}$$

When the coupling parameters yield rhythmic firing (i.e., power spectrum of the population firing rate is not flat), the net synaptic input is large on average (averaged over time and across excitatory neurons) and is much larger than when the network is in an asynchronous regime. Thus, we consider the large firing rate limit in the reduced theoretical description (15)–(16). Furthermore, we ignore the effects of the refractory period τ_{ref} [3], external noise $\tilde{\eta_E}$, and focus on the formula for the deterministic firing rate (15):

$$\tau_m r_0(q,\theta) = \frac{1+qx_0}{\log\left(\frac{qx_1}{qx_1-\theta(1+qx_0)}\right)} \tag{21}$$

We assume the random state variables are parameters just like in the reduced description, which will enable us to focus on (q,θ) and determine how these two parameters effect the firing rate range. The two vectors $(\mathbf{q},\boldsymbol{\theta})$ are the main source of the firing rate heterogeneity. The large firing rate regime is captured by a series expansion of log() around 1. Standard asymptotic calculations enable equation (21) to be re-written as:

$$\tau_m r_0(q,\theta) = \frac{1+qx_0}{\log\left(\frac{qx_1}{qx_1-\theta(1+qx_0)}\right)} \tag{22}$$

$$= \frac{q}{\theta}x_1 - \frac{1}{2}(1+qx_0) - \frac{(1+qx_0)^2\theta}{12[qx_1-\theta(1+qx_0)]} + O\left(z^2(1+qx_0)\right) \tag{23}$$

$$\text{where } z := \theta\frac{1+qx_0}{qx_1-\theta(1+qx_0)} \tag{24}$$

The modulation of the firing rate heterogeneity can be understood simply by the dominant term (i.e., first term):

$$\frac{q}{\theta}x_1; \tag{25}$$

specifically, the fraction q/θ is key because the second factor x_1 does not vary much as the correlation between $\mathbf{q}$ and $\boldsymbol{\theta}$ changes.

[3] Although ignoring the refractory period could be problematic for large firing rates, we emphasize that the value of our analysis is not in quantitative matching of simulations but rather for a deeper understanding of how network attributes effect the outputs. A similar calculation has been performed with the refractory period (not shown), but the asymptotic formulas are not insightful.

In the rhythmic firing regime, the modulation of the range of firing rates can be understood simply with range of values given by the fraction q_j/θ_j. Specifically, the ratio $q_j \frac{1}{\theta_j}$ yields N_e values, and the range of these values for a particular parameter is indicative of the relative range of firing rates. In this regime (rhythmic firing) when $\varrho(\mathbf{q}, \boldsymbol{\theta}) < 0$, the extreme values consists of: i) larger q_j values that tend to occur with smaller θ_j values, resulting in an amplification (and relatively larger) $q\frac{1}{\theta}$ for the upper range of values, and ii) smaller q_j values and larger θ_j, resulting in an overall smaller (small times small) values to account for the lower range of $q\frac{1}{\theta}$ values. When $\varrho(\mathbf{q}, \boldsymbol{\theta}) > 0$, similar reasoning applies to larger q_j values tending to occur with larger θ_j values (large times small) and smaller values (small times large), resulting in a diminished range of $q\frac{1}{\theta}$ values than when $\varrho > 0$. Note that the mean of q_j/θ_j (across the N_e population) is approximately constant as ϱ varies (not shown).

A side-by-side comparison shows how similar the dynamics are (Fig. 5A–B, E–F) and is validation that the range of excitatory firing rates is driven by this factor $(\mathbf{q}/\boldsymbol{\theta})$. Figure 5 compares the excitatory firing rate range of the LIF simulations (left column) to the analytic descriptions (right column, sections 3.2–3.3) as a function of $\varrho(\mathbf{q}, \boldsymbol{\theta})$ for two fixed levels of heterogeneity: $\sigma_q = \sigma_\theta = 1$ (black) and $\sigma_q = \sigma_\theta = 0.44$ (dark orange). Of course we do not expect precise quantitative matching between the analytic description (Fig. 5 right column) and the actual network simulation (Fig. 5 left column) because the analysis had many assumptions meant to highlight a proof of principle. Nevertheless, the theory is quite descriptive and captures the general trend (the values of equation (25) are shown in Fig. 5B,F for completeness). Therefore, in the rhythmic firing regime, q/θ compactly describes how when intrinsic and network heterogeneity are anti-correlated the range of firing rates is larger than when they are correlated.

3.3 Analytic description of heterogeneous firing rate range in asynchronous networks

For the asynchronous regime, the range of firing rates actually increases as the correlation between $\boldsymbol{\theta}$ and $\mathbf{q}$ increases (Fig. 3D), which is the opposite trend compared to when the network is firing rhythmically (Fig. 2D and 4D). This section provides an analytic description for this phenomena.

In contrast to when the population firing rate is rhythmic, the asynchronous regime (i.e., power spectrum of population firing rate is flat) has much less net synaptic input on average. Therefore, we cannot ignore the noise variable $\tilde{\eta_E}$ and must consider a different regime than in the previous section. Here, the refractory period τ_{ref} is ignored, and all of the random variables are again assumed to be parameters *except* the noise variable $\tilde{\eta_E}$ because of how crucial it is for firing in this regime. The formula for the reduced firing rate is (cf. equations (16) and (21)):

$$\tau_m r_0(q,\theta) = \frac{1+qx_0}{\sigma_E\sqrt{\pi}} \int \left\lceil \frac{1}{\log\left(\frac{qx_1+\tilde{\eta_E}}{qx_1+\tilde{\eta_E}-\theta(1+qx_0)}\right)} \right\rceil^+ e^{-\tilde{\eta_E}^2/\sigma_E}\, d\tilde{\eta_E} \tag{26}$$

where $\lceil\ \rceil^+$ represents thresholding: if $\tilde{\eta_E} \leq \theta(1+qx_0) - qx_1$ it is 0, otherwise it is $1/\log(\cdot)$. This equation can be re-written by substituting $\lceil 1/\log(\cdot)\rceil^+$ with an integral, and interchanging the order of integration:

$$\begin{aligned}\tau_m r_0(q,\theta) &= \frac{1+qx_0}{\sigma_E\sqrt{\pi}} \int_{-\infty}^{\infty} \int_{qx_1+\tilde{\eta_E}-\theta(1+qx_0)}^{qx_1+\tilde{\eta_E}} M(y)\, dy e^{-\tilde{\eta_E}^2/\sigma_E}\, d\tilde{\eta_E} \\ &= \frac{1+qx_0}{\sigma_E\sqrt{\pi}} \int_{-\infty}^{\infty} \int_{y-qx_1}^{y-qx_1+\theta(1+qx_0)} e^{-\tilde{\eta_E}^2/\sigma_E}\, d\tilde{\eta_E} M(y)\, dy \end{aligned} \tag{27}$$

where $M(y)$ is an antiderivative of $\lceil 1/\log(\cdot)\rceil^+$. In the asynchronous firing regime, the modulation of the range of firing rates can be understood simply with the last term of upper limit of the inner integral:

$$\theta(1+qx_0) \tag{28}$$

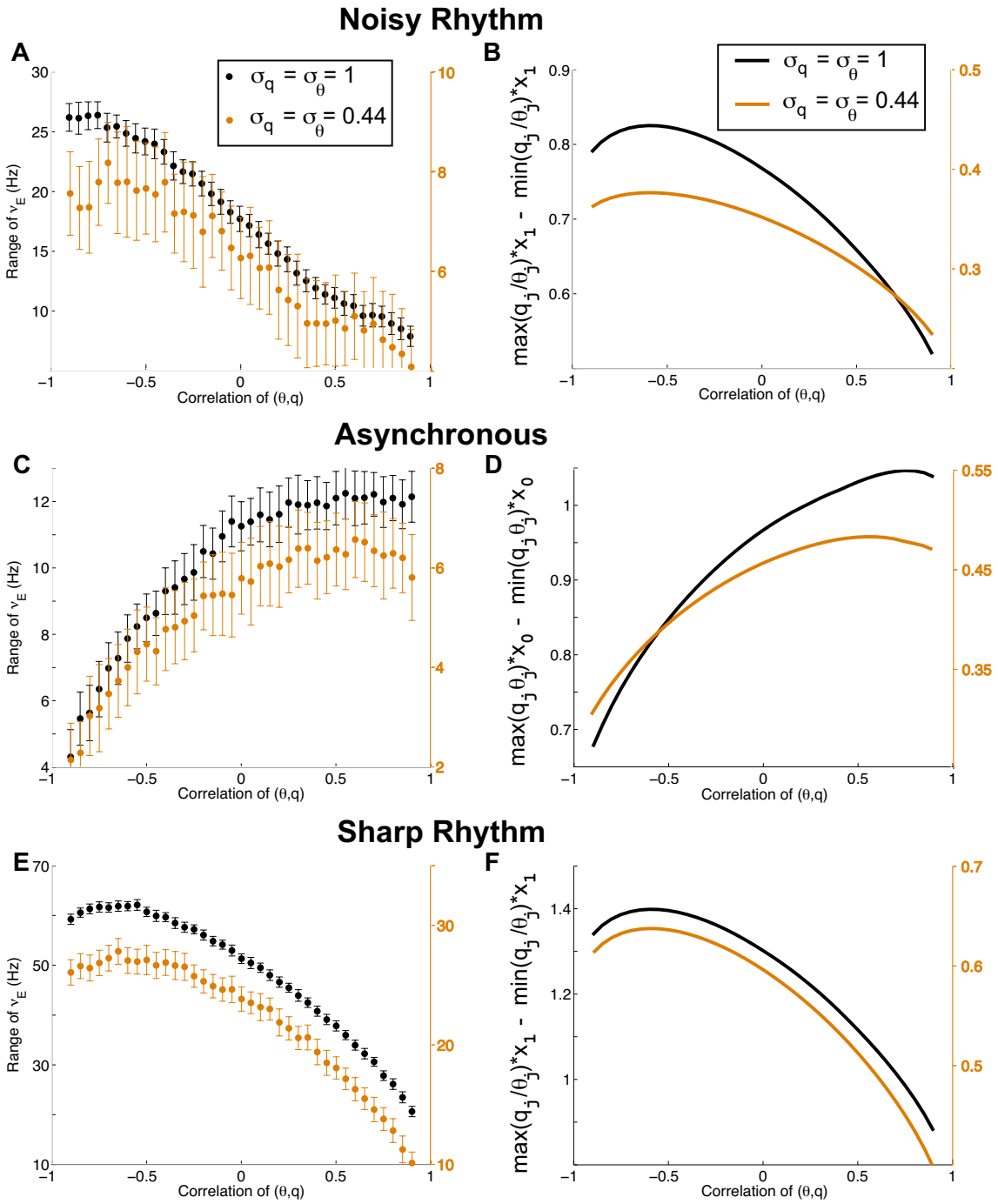

Fig. 5 Analytic description of excitatory firing rate ranges. Here, the firing rate ranges are for a fixed level of heterogeneity $\sigma_q = \sigma_\theta$ and different correlation $\varrho(\mathbf{q}, \boldsymbol{\theta})$ values. A)–B) Noisy Rhythm regime: the range of firing rates for the completely heterogeneous ($\sigma_q = \sigma_\theta = 1$, black dots) network and with less heterogeneity ($\sigma_q = \sigma_\theta = 0.44$, dark orange dots) are plotted as the correlation varies on the same axis (see left and right vertical axes for respective scales). B) The theory in section 3.2 provides an analytic description (see (25)) for how the correlation of intrinsic and network heterogeneity lead to relatively different firing rate ranges in this regime. As the correlation ϱ increases, the range of firing rates tends to decrease. C)–D) Asynchronous regime: similar to A)–B), but the reduction theory in D) is in section 3.3, again providing an analytic description (see (28)) for how the range of firing rates increases as the correlation ϱ increases. E)–F) Sharp Rhythm regime: similar to A)–B), using the same analytic description. The analytic descriptions in the right column (B, D, F) use x_0 and x_1 (see (19)–(20)) values obtained from $\varrho = 0$. Error bars in A, C, and E are estimates of the standard deviation about the sample mean of the range (see last paragraph of Section 2.1 for details).

because the other pieces of r_0 do not vary much across the N_e neurons. Furthermore, since the focus is on understanding the range of firing rates as determined by the correlation of $(\mathbf{q}, \boldsymbol{\theta})$, then the product: θq is what determines the relative change in the range (like before, x_0 does not change much across the excitatory neurons). This is in sharp contrast to equation (25), where the intrinsic heterogeneity θ divides the network heterogeneity q. Figure 5C–D shows that the analytic description (28) clearly captures the trend in the range of firing rates as ϱ changes.

These formulas (25), (28), clearly show how the two forms of heterogeneity $(\mathbf{q}, \boldsymbol{\theta})$ effect one another to yield the different trends in the range of firing rates in different regimes. Simply put, in the rhythmic regime, the relationship q/θ determines how the range of the firing rates change while in the asynchronous regime, $q\theta$ determines this; note that plotting q/θ and $q\theta$ without x_0 and x_1 does not appreciably change the shape of the curves in Figure 5 (not shown).

The key to our analysis was to focus on the main sources of heterogeneity, and therefore the firing rate heterogeneity, in a proper framework (probability density functions) to describe the essence of how the firing rate range changes. This analysis was successful partly because the heterogeneity (q, θ) drove the changes in the firing rate range, as opposed to other factors such as external noise, etc., and our analysis centered on these parameters.

4 Discussion

We studied how two forms of heterogeneity: intrinsic and network, effect the (excitatory) firing rate distribution of a recurrently coupled stochastic network of leaky integrate-and-fire neurons. Since the relationship between intrinsic and network heterogeneity is not known (to the best of our knowledge), we systematically varied the relationship or correlation to assess the effects on the network in different regimes. This work showed how the firing rate range changes with the correlation of intrinsic and network heterogeneity: in the rhythmic or oscillatory regime, the firing rate range tends to decrease with increasing correlation (i.e., when larger firing thresholds tend to have larger synaptic input amplification), while the opposite trend is observed in the asynchronous regime. These observations were captured by the analytic descriptions in equations (25) and (28). We also found that the firing rate ranges can be relatively large or small depending on the correlation between intrinsic and network heterogeneity, thus the overall level of heterogeneity can be mitigated or amplified depending on this relationship. If the relationship between intrinsic and network heterogeneity could be measured in a cortical network, these results would enable predictions for the range of response heterogeneity. Although we chose to analyze two specific forms of heterogeneity in a theoretical model, connections to experimental recordings of heterogeneity and firing rates may be possible even with related neural attributes (i.e., the membrane time constant as a proxy for firing threshold, or relating network connectivity to input variability). Also, the framework presented here could in principle be adapted to other heterogeneous neural attributes that would naturally require augmentations.

Marder (2011) showed how combining intrinsic and synaptic conductance heterogeneity could lead to similar outputs, depending on their relationship. Their work was naturally different than the work here: different parameters were varied and the underlying neuron model had ionic currents and specific circuitry motivated by the crustacean stomatogastric ganglion. Also, they were interested in the rhythmic output of the network rather than characterizing the range of the population response heterogeneity. The results in Marder (2011) are similar in spirit to what has been shown here in that different sets of parameters can result in similar output (also see Marder and Goaillard (2006)); in our case, the range of excitatory firing rates can arise with different levels of heterogeneity by tuning the correlation between the two sources of heterogeneity. One of the conclusions of their work is that the intrinsic and network parameters, or heterogeneities, must be taken as a whole and the correlation among these parameters is crucial in determining network output. Our study compliments these assertions in a specific way, by determining how the correlation of two parameters alters the range of the excitatory firing rates in different regimes.

Unlike the work of Hermann and Touboul (2012); Mejias and Longtin (2012), we do not consider how synaptic heterogeneity can induce different dynamics but rather focus on specific spiking regimes that are similar with and without heterogeneities. Their work has a more detailed characterization of the dynamics, whereas our work explores the effects of two specific forms of heterogeneities away from the bifurcation points. Studying how the relationship of intrinsic and network heterogeneity induces different dynamics would be interesting but is beyond the scope of this paper. A recent paper of Ostojic (2014) calls the first regime that we termed noisy rhythm 'a second type of asynchronous' network but with stronger coupling. Ostojic (2014) found that these two types of asynchronous networks (classic and strongly coupled) processed external stimuli differently, a feature that was not considered in this paper. These two regimes (Ostojic's strongly asynchronous regime and the noisy rhythm here) are similar because the coupling is relatively strong and both autocorrelation functions of the population firing rates are similar. Consistent with illustrating that these regimes are different, we have shown how the classic asynchronous regime is different than the noisy rhythm or 'strongly coupled asynchronous' (Ostojic) because the firing rate ranges change in distinct ways.

A related study analyzes the interplay of two sources of intrinsic heterogeneity (Mejias and Longtin, 2014); specifically, Mejias and Longtin (2014) studied how heterogeneity in the excitatory and inhibitory spiking thresholds had different effects on a coupled network (LIF with excitatory and inhibitory neurons). They found distinct roles for heterogeneity in each type of neuron: excitatory heterogeneity can increase firing rate and linearizes output response, inhibitory heterogeneity can decrease network response and lead to gain control of input/output response (see Mejias and Longtin (2014) for further details). Their analysis also characterized the heterogeneity-induced transitions from asynchrony to synchrony and briefly considered the combined effects of these two attributes. Our work only considered excitatory heterogeneity; the effects of inhibitory neuron heterogeneity combined with network heterogeneity are not known and a potential future direction of research. Another study by Hunsberger et al (2014) examined how varying both (white) noise in the voltage and heterogeneity in the threshold for firing led to different information (mutual information) content in spiking neuron models (LIF and Fitzhugh-Nagumo). They found an optimal level of heterogeneity for maximizing information content for a fixed level of noise (and for fixed level of heterogeneity there was an optimal level of noise, i.e., a stochastic resonance). Their results are distinct from Mejias and Longtin (2012) and Tripathy et al (2013) (who also found optimal information by tuning parameters) because they considered the interplay of those two sources of variability and determined that they interact nonlinearly (e.g., the optimal parameters are different with both components). In our study, we did not systematically analyze how varying the (correlated) noise level σ_E and heterogeneity effect network statistics. Hunsberger et al (2014) explained their simulation results by comparing how each component desynchronized and/or linearized the network response properties, whereas we provide an analytic explanation. Finally, Lengler et al (2013) recently simulated an LIF network with a large number of heterogeneous intrinsic and network parameters. They find that heterogeneity can increase response time and paradoxically less variable responses (reliability), though they do not provide underlying mechanistic explanations for their results.

Our study provides a more complete understanding of how heterogeneities interact and result in modulation of the firing rate statistics, which may ultimately lead to a better understanding of neural coding in coupled neural networks. Even though the firing rate is a first order measure of the response statistics, the range of this quantity has an impact on coding. There have been a number of recent studies focusing on the impact of heterogeneity on neural coding. Padmanabhan and Urban (2010) showed with recordings of mitral cells in mice olfactory bulb that heterogeneous cells had lower correlated activity, which is thought to increase information capacity of a given population. Similarly, Chelaru and Dragoi (2008) found diverse orientation tuning curves enhances coding with increased information via a reduction in correlated activity of a coupled LIF network. Shamir and Sompolinsky (2006) proposed a theoretical explanation for the benefits of diversity/heterogeneity in population coding, whereby the information capacity is not limited to the correlation of activity. A future direction of study is how different forms of heterogeneities considered in this paper lead to changes in the second order statistics (correlation or co-variability), which also have implications for coding in neural systems. Although many

of the previous studies conclude that heterogeneity generally leads to lower co-variability (Chelaru and Dragoi, 2008; Padmanabhan and Urban, 2010), better discrimination (Marsat and Maler, 2010; Mejias et al, 2013), and ultimately enhanced coding, the subtleties of how co-variability is modulated is not completely known and remains an active area of research (Ponce-Alvarez et al, 2013; Ruff and Cohen, 2014; Mochol et al, 2015).

Acknowledgements We thank Gary Marsat and Brent Doiron for enlightening conversations, and Brent Doiron for providing feedback on the manuscript. This work was supported by a grant from the Simons Foundation (#355173, Cheng Ly).

Appendix: Generating correlated q and $\boldsymbol{\theta}$

Given two vectors $\boldsymbol{\theta}$ (intrinsic heterogeneity) and $\mathbf{q}$ (network heterogeneity), we can generate a new pair of vectors (of the same size) that have any desired correlation coefficient $\varrho \in (-1, 1)$. In this paper, we choose to keep $\mathbf{q}$ fixed and generate a new vector $\boldsymbol{\vartheta}$ that has the same sample mean ($\mu(\boldsymbol{\theta})$) and sample standard deviation ($\sigma(\boldsymbol{\theta})$) of $\boldsymbol{\theta}$. Note that there are infinitely many ways to generate two such vectors if we only require that the mean and standard deviation of the new vectors be equal to the original statistics of the vector. The algorithm we use is as follows.

- INPUTS: $(\mathbf{q}, \boldsymbol{\theta}, \varrho)$
- Set $\varphi = \cos^{-1}(\varrho)$
- Shift input vectors so they have zero mean:
  $\mathbf{q}_0 = \mathbf{q} - \mu(\mathbf{q})$
  $\boldsymbol{\theta}_0 = \boldsymbol{\theta} - \mu(\boldsymbol{\theta})$.
- Calculate orthogonal complement to $\mathbf{q}_0$:
  $\mathbf{z} = \boldsymbol{\theta}_0 - \frac{\mathbf{q}_0 \cdot \boldsymbol{\theta}_0}{\|\mathbf{q}_0\|^2}\mathbf{q}_0$
- Create unit vectors out of $\mathbf{q}_0$ and $\mathbf{z}$:
  $\tilde{\mathbf{q}} = \mathbf{q}_0/\|\mathbf{q}_0\|$, $\tilde{\mathbf{z}} = \mathbf{z}/\|\mathbf{z}\|$
- Create vector with prescribed correlation and zero mean:
  $\hat{\boldsymbol{\theta}} = \cos(\varphi)\tilde{\mathbf{q}} + \sin(\varphi)\tilde{\mathbf{z}}$
- Set $\boldsymbol{\vartheta} = \frac{\sigma(\boldsymbol{\theta})}{\sigma(\hat{\boldsymbol{\theta}})}\hat{\boldsymbol{\theta}} + \mu(\boldsymbol{\theta})$
- OUTPUT: $\boldsymbol{\vartheta}$, where correlation coefficient of $\boldsymbol{\vartheta}$ and $\mathbf{q}$ is ϱ, $\mu(\boldsymbol{\vartheta}) = \mu(\boldsymbol{\theta})$, and $\sigma(\boldsymbol{\vartheta}) = \sigma(\boldsymbol{\theta})$.

References

Apfaltrer F, Ly C, Tranchina D (2006) Population density methods for stochastic neurons with realistic synaptic kinetics: Firing rate dynamics and fast computational methods. Network: Computation in Neural Systems 17:373–418

Börgers C, Kopell N (2003) Synchronization in networks of excitatory and inhibitory neurons with sparse, random connectivity. Neural computation 15(3):509–538

Bremaud A, West D, Thomson A (2007) Binomial parameters differ across neocortical layers and with different classes of connections in adult rat and cat neocortex. Proceedings of the National Academy of Sciences 104:14,134–14,139

Burton S, Ermentrout B, Urban N (2012) Intrinsic heterogeneity in oscillatory dynamics limits correlation-induced neural synchronization. Journal of Neurophysiology 108:2115–2133

Buzsáki G, Wang XJ (2012) Mechanisms of gamma oscillations. Annual review of neuroscience 35:203

Chelaru M, Dragoi V (2008) Efficient coding in heterogeneous neuronal populations. Proceedings of the National Academy of Sciences 105:16,344–16,349

Chow CC (1998) Phase-locking in weakly heterogeneous neuronal networks. Physica D: Nonlinear Phenomena 118:343–370

Economo MN, White JA (2012) Membrane properties and the balance between excitation and inhibition control gamma-frequency oscillations arising from feedback inhibition. PLoS computational biology 8(1):e1002,354

Haskell E, Nykamp DQ, Tranchina D (2001) Population density methods for large-scale modeling of neuronal networks with realistic synaptic kinetics: cutting the dimension down to size. Network: Compututation in Neural Systems 12:141–174

Hermann G, Touboul J (2012) Heterogeneous connections induce oscillations in large-scale networks. Physical Review Letters 109:018,702

Hertäg L, Durstewitz D, Brunel N (2014) Analytical approximations of the firing rate of an adaptive exponential integrate-and-fire neuron in the presence of synaptic noise. Frontiers in computational neuroscience 8

Hunsberger E, Scott M, Eliasmith C (2014) The competing benefits of noise and heterogeneity in neural coding. Neural computation 26(8):1600–1623

Lengler J, Jug F, Steger A (2013) Reliable neuronal systems: The importance of heterogeneity. PloS one 8(12):e80,694

Levy RB, Reyes AD (2012) Spatial profile of excitatory and inhibitory synaptic connectivity in mouse primary auditory cortex. The Journal of Neuroscience 32(16):5609–5619

Ly C (2013) A Principled Dimension Reduction Method for the Population Density Approach to Modeling Networks of Neurons with Synaptic Dynamics. Neural Computation 25:2682–2708

Ly C (2014) Dynamics of coupled noisy neural oscillators with heterogeneous phase resetting curves. SIAM Journal on Applied Dynamical Systems 13:1733–1755

Ly C, Tranchina D (2009) Spike Train Statistics and Dynamics with Synaptic Input from any Renewal Process: A Population Density Approach. Neural Computation 21:360–396, DOI 10.1162/neco.2008.03-08-743

Ly C, Middleton J, Doiron B (2012) Cellular and circuit mechanisms maintain low spike co-variability and enhance population coding in somatosensory cortex. Frontiers in Computational Neuroscience 6:1–26, DOI 10.3389/fncom.2012.00007

Marder E (2011) Variability, compensation, and modulation in neurons and circuits. Proceedings of the National Academy of Sciences 108:15,542–15,548

Marder E, Goaillard J (2006) Variability, compensation and homeostasis in neuron and network function. Nature Reviews Neuroscience 7:563–574

Markram H, Lübke J, Frotscher M, Roth A, Sakmann B (1997) Physiology and anatomy of synaptic connections between thick tufted pyramidal neurones in the developing rat neocortex. The Journal of Physiology 500:409

Marsat G, Maler L (2010) Neural heterogeneity and efficient population codes for communication signals. Journal of neurophysiology 104:2543–2555

Mejias J, Longtin A (2012) Optimal heterogeneity for coding in spiking neural networks. Physical Review Letters 108:228,102

Mejias J, Longtin A (2014) Differential effects of excitatory and inhibitory heterogeneity on the gain and asynchronous state of sparse cortical networks. Frontiers in computational neuroscience 8

Mejias JF, Marsat G, Bol K, Maler L, Longtin A (2013) Learning contrast-invariant cancellation of redundant signals in neural systems. PLoS computational biology 9(9):e1003,180

Mochol G, Hermoso-Mendizabal A, Sakata S, Harris KD, de la Rocha J (2015) Stochastic transitions into silence cause noise correlations in cortical circuits. Proceedings of the National Academy of Sciences 112(11):3529–3534

Moreno-Bote R, Parga N (2006) Auto- and Crosscorrelograms for the Spike Response of Leaky Integrate-and-Fire Neurons with Slow Synapses. Physical Review Letters 96:028,101

Nesse WH, Borisyuk A, Bressloff P (2008) Fluctuation-driven rhythmogenesis in an excitatory neuronal network with slow adaptation. Journal of Computational Neuroscience 25:317–333

Nicola W, Ly C, Campbell SA (2015) One-dimensional population density approaches to recurrently coupled networks of neurons with noise. SIAM Journal on Applied Mathematics (in press):–

Nykamp D, Tranchina D (2001) A Population Density Approach That Facilitates Large-Scale Modeling of Neural Networks: Extension to Slow Inhibitory Synapses. Neural Computation 13:511–546

Ostojic S (2014) Two types of asynchronous activity in networks of excitatory and inhibitory spiking neurons. Nature neuroscience 17:594–600

Ostojic S, Brunel N, Hakim V (2009) Synchronization properties of networks of electrically coupled neurons in the presence of noise and heterogeneities. Journal of Computational Neuroscience 26(3):369–392

Oswald A, Doiron B, Rinzel J, Reyes A (2009) Spatial profile and differential recruitment of gabab modulate oscillatory activity in auditory cortex. The Journal of Neuroscience 29:10,321–10,334

Padmanabhan K, Urban N (2010) Intrinsic biophysical diversity decorrelates neuronal firing while increasing information content. Nature Neuroscience 13:1276–1282

Parker D (2003) Variable properties in a single class of excitatory spinal synapse. The Journal of neuroscience 23(8):3154–3163

Ponce-Alvarez A, Thiele A, Albright T, Stoner G, Deco G (2013) Stimulus-dependent variability and noise correlations in cortical mt neurons. Proceedings of the National Academy of Sciences 110:13,162–13,167

Ruff DA, Cohen MR (2014) Attention can either increase or decrease spike count correlations in visual cortex. Nature neuroscience 17(11):1591–1597

Shamir M, Sompolinsky H (2006) Implications of neuronal diversity on population coding. Neural Computation 18:1951–1986

Strogatz SH, Mirollo RE (1991) Stability of incoherence in a population of coupled oscillators. Journal of Statistical Physics 63:613–635

Tripathy S, Padmanabhan K, Gerkin R, Urban N (2013) Intermediate intrinsic diversity enhances neural population coding. Proceedings of the National Academy of Sciences 110:8248–8253

Wang XJ (2010) Neurophysiological and computational principles of cortical rhythms in cognition. Physiological reviews 90:1195–1268

Xue M, Atallah BV, Scanziani M (2014) Equalizing excitation-inhibition ratios across visual cortical neurons. Nature 511:596–600

Yim M, Aertsen A, Rotter S (2013) Impact of intrinsic biophysical diversity on the activity of spiking neurons. Physical Review E 87:032,710